AIAA JOURNAL
Vol. 34, No. 11, November 1996

Counterflow Thrust Vectoring of Supersonic Jets

P. J. Strykowski*
University of Minnesota, Minneapolis, Minnesota 55455
and
A. Krothapalli† and D. J. Forliti‡
Florida A&M University and Florida State University, Tallahassee, Florida 32316

Fluidic thrust vector control is examined in a supersonic rectangular jet having a 4:1 aspect ratio and for jet stagnation temperatures between 300 and 670 K. Experiments conducted in a nominally ideally expanded Mach 2 jet reveal that thrust can be continuously vectored up to at least 16 deg by creating a secondary counterflowing stream between the primary jet and an adjacent curved surface. Thrust vector control using counterflow is shown to be effective in both cold and moderately heated supersonic jets and to perform free of bistable or hysteretic effects. Measurements indicate that proportional thrust vector control can be achieved with less than 4% thrust loss and requiring secondary mass flow rates less than approximately 2% of the primary jet.

Nomenclature

a_1 = sound speed in primary stream
a_2 = sound speed in secondary stream
C = transverse collar height
C_T = thrust coefficient
G = counterflow gap height
H = short exit dimension of jet
L = collar extension length
M_c = convective Mach number
$\dot{m}_1$ = mass flow rate in primary stream
$\dot{m}_2$ = mass flow rate in secondary stream
$\hat{P}$ = dimensionless gap pressure
P_c = collar static pressure (gauge)
P_G = static pressure in counterflow gap (gauge)
R = collar radius of curvature
R_x = resultant axial force
R_y = resultant side force
T_o = jet stagnation temperature in primary stream
V_1 = primary jet exit velocity
V_2 = counterflow velocity
$|V_2|$ = magnitude of velocity vector in secondary stream
W = long exit dimension of jet
x = streamwise coordinate
α = collar turning angle
δ_v = effective thrust vector angle
ρ_1 = density in the primary stream
ρ_2 = density in the secondary stream

Introduction

RECENT flight tests of both two-dimensional pitch vectoring and multiaxis vectoring nozzles have demonstrated the viability of aircraft control schemes based on advanced jet exhaust technologies. The inherent advantages of thrust vector systems over traditional flight control include poststall performance, the ability to operate on damaged airfields by virtue of reduced takeoff distances, and overall enhanced agility including superior roll characteristics. Current exhaust nozzles capable of vectoring thrust require movable control surfaces to redirect the jet exhaust. Although these mechanical-based strategies have proven effective in multiaxis applications and have exhibited external drag characteristics quite comparable to nonvectored nozzles, there remain a number of unresolved issues, including weight and transient response, that have focused renewed attention on fluidic-based strategies for vectoring thrust. Fluidic thrust vector control has the potential advantage over existing technologies in that the control surfaces are stationary, considerably reducing the complex actuation and control hardware required to vector thrust using conventional mechanical means.

We will describe one such approach, which employs a secondary counterflowing stream to develop the nozzle pressure distribution necessary for thrust vectoring. In addition to the benefits of fluidic control such as reduced weight and mechanical support, counterflow thrust vectoring has the potential advantage of isolating the control surfaces from direct exposure to the high-temperature exhaust gases, thereby reducing the observability of the nozzle and the need for an independent cooling system. Counterflow thrust vectoring attempts to combine the proportional vector control of mechanical-based systems with the simplicity of fluidic control. However, surveying the literature it is apparent that fluidic control is not without its difficulties, the most serious of which is the hysteretic nature of these devices, which can give rise to the attachment of the jet to adjacent surfaces and catastrophic loss of control. Consequently, the viability of any fluidic-based strategy must examine the presence of hysteretic effects over the entire operating domain in which the system must function.

The advantages of thrust vector control have been demonstrated under flight conditions using two-dimensional nozzles employing pitch vectoring as well as in axisymmetric configurations where multiaxis capabilities were of primary concern.[1,2] Flight tests successfully illustrated the benefits of vector control, displaying reduced takeoff roll and significant improvements in pitch rate. Early attempts to achieve multiaxis thrust vector control were based on strategies successfully developed for pitch vectoring systems, namely, by the relatively simple mechanical actuation of flaps or vanes. For instance, three-vane multiaxis designs were used to achieve increased roll rates and enhanced maneuverability at low speeds and at high angles of attack. Recent multiaxis nozzle designs have incorporated more elaborate vane hardware capable of achieving full pitch and yaw control in axisymmetric configurations while maintaining the external drag levels of nonvectoring systems.[2,3]

The use of fluidic elements to control high-speed jet behavior is not new, having received considerable attention several decades ago due to the attractive bistable characteristics of these devices in logic applications.[4-6] However, the hysteretic nature of fluidic amplifiers, which makes them ideal for decision making, also renders them quite undesirable for aircraft control applications where a unique

Received April 20, 1996; revision received July 29, 1996; accepted for publication July 31, 1996; also published in *AIAA Journal on Disc*, Volume 2, Number 1.

*Associate Professor, Department of Mechanical Engineering. Member AIAA.
†Don Fuqua Professor and Chairman, Department of Mechanical Engineering. Associate Fellow AIAA.
‡Graduate Research Assistant, Department of Mechanical Engineering. Member AIAA.

and proportional operating curve is essential. Several fluidic-based thrust vector systems have overcome these control issues, at least over limited portions of the operating domain.[7-9] Typical strategies involve single or multiport injection of secondary flow into the jet exhaust to affect changes in the vectored thrust. One potential limitation of fluid injection schemes is the rather large secondary mass flow requirements needed for actuation.

In addition to variable geometry and fluidic nozzles, various other schemes for thrust vector control have been explored. One notable study is that of Parekh et al.[10] This study placed low-power piezoelectric actuators at the exit of the long dimension of a moderate aspect ratio rectangular nozzle. A thin sheet of steel, sandwiched between the piezoelectric material, was vibrated parallel to the jet exit to excite the shear layer on one side of the jet, leading to flow turning in that direction. This effect was achieved with little increase in cross-stream spreading but has been limited at this time to subsonic applications. Still another method is the use of translating side walls of underexpanded nozzles as researched by Cornelius and Lucius.[11] This method employs a simple extension of a side wall on an underexpanded nozzle. Results indicated that a 20-deg vector angle in one direction was achievable for both two-dimensional and three-dimensional nozzle designs with little penalty in thrust performance. Finally, the work of Wallace and Redekopp[12] examines thrust vectoring in two-dimensional jets by disturbing the symmetry of the jet profile.

Fluidic Counterflowing Nozzle

The fluidic nozzle concept employed in the present investigation is shown schematically in Fig. 1 and illustrates the side view of the short dimension of a 4:1 aspect ratio rectangular jet. Curved surfaces called collars are placed on either side of the primary flow nozzle (top and bottom in the figure) creating gaps between the exhausting jet and the collar surfaces, which are curved away from the jet axis in the streamwise direction. To achieve upward thrust vectoring at an angle δ_v, as shown in Fig. 1, a secondary counterflow must be established between the primary jet and the collar surface creating a continuous flow path between the surrounding ambient fluid and the vacuum system. Parallel side plates attached to the collar are used to isolate the secondary flow to either the upper or lower shear layers and minimize three-dimensional effects.

Anticipating the results to follow, it appears that the operation of the fluidic thrust vector nozzle shown in Fig. 1 depends on the shear layer entrainment characteristics of the two opposing shear layers, which give rise to markedly different pressure distributions on the upper and lower collars during vectoring. This conjecture is based on studies showing that the mixing and entrainment characteristics of countercurrent mixing layers are augmented relative to the more common coflowing arrangement for the same level of shear,[13-15] providing a mechanism for the enhanced cross-stream momentum transport and pressure gradient in the presence of the collar surface. We will explore this connection in the sections to follow after the basic operation of the fluidic counterflowing nozzle is described.

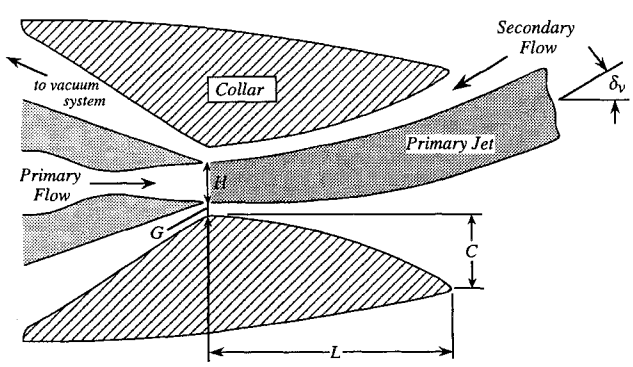

Fig. 1 Schematic of fluidic thrust vector nozzle showing vectoring when counterflow is activated in the upper shear layer of the jet.

Facilities

The experiments were conducted in the blowdown compressed air facility of the Fluid Mechanics Laboratory located at Florida State University. The facility is driven by a high-displacement reciprocating air compressor, which is capable of supplying air at a maximum storage pressure of 160 bars; intercoolers are used to reduce the water vapor content of the air. Large storage tanks provide a total capacity of 10 m^3 and are capable of driving the Mach 2 primary jet flow examined in this study continuously for up to 30 min. After leaving the storage tanks, the air can be heated by passing through an array of resistive tank heaters having a maximum power output of 450 kW and capable of achieving stagnation temperatures in excess of 750 K. Operating the facility at elevated stagnation temperatures requires preheating the facility downstream of the tank heaters. This process bleeds the storage tanks somewhat, but the overall run time is not significantly affected because the mass flow rate at a fixed Mach number is reduced with increasing stagnation temperature. The stagnation pressure was held invariant to within 0.5% during each experiment using staged control valves.

For the present study the blowdown facility was fitted with a rectangular nozzle having an exit aspect ratio of 4:1. The dimensions of the nozzle in the exit plane measured $H = 13.0$ mm by $W = 52.0$ mm and the throat area was 400 mm^2. The contour of the short dimension of the nozzle was generated by a method of characteristics for a design Mach number of 2.0. The walls of the long dimension of the nozzle were parallel downstream of the throat and were blended to facilitate a transition from the rectangular cross section to the circular dimension of the connecting pipe upstream of the throat. During all experiments the stagnation to ambient pressure ratio was held at nominally 7.82 as required for isentropically expanded flow at Mach 2. The jet was operated cold at a stagnation temperature of 300 K, corresponding to an exit plane Reynolds number of 1.23×10^6 based on the short dimension of the jet. Hot supersonic flow was studied by elevating the stagnation temperature to 670 K, which produced a lower exit Reynolds number of 0.43×10^6.

As illustrated in Fig. 1, a secondary stream is developed using a vacuum source that can be independently connected to create counterflow in the upper or lower shear layer of the jet. The mass flow rate of the secondary stream was obtained by integrating the velocity profile within the supply line leading to the vacuum system. The counterflow slot height was varied in the present experiments between 3.5 and 9.5 mm, corresponding to $0.27 \leq G/H \leq 0.73$, and the collars were placed symmetrically about the jet centerline. The inner contour of the collar was an arc of constant radius of curvature swept through an angle α and extending downstream of the nozzle exit a distance given by $L = R \cdot \sin \alpha$. The maximum lateral extent of the inner collar can be evaluated as $C = R \cdot (1 - \cos \alpha)$. The geometry considered in the present study is drawn to scale in Fig. 1 and corresponds to $L/H = 6.9$ and $R/H = 15.7$, where $\alpha \approx 26$ deg. Fifteen pressure taps were positioned at equal intervals along the collar surface to capture the static pressure in the streamwise direction. The first streamwise tap at $x = 0$ was used to reference the conditions in the gap of the counterflowing stream and is expressed as P_G. (The pressures P_c and P_G will be indicated in gauge pressures. The streamwise coordinate is given by x, which has its origin in the jet exit plane and is measured positively in the direction of the primary jet.) Static pressures were scanned with a Validyne differential pressure transducer (model DP-15) and digitized using an RC Electronics ISC-16 A/D converter. Averages taken over a period of 10 s provided an uncertainty in pressure of ± 2 mbar, which includes the signal unsteadiness (i.e., first-order uncertainty analysis).

Visualization of the jet was achieved by creating laser sheet images of the vectored plane along the jet axis using a pair of Spectra Physics frequency doubled Nd:YAG pulsed lasers. The lasers were fired simultaneously with a pulse energy of approximately 90 mJ each and a pulse width of 5 ns. Fine condensation particles formed in the mixing region between the cold air of the primary jet and the moist ambient air were used for light scattering in a technique described by Clemens and Mungal[16] and captured on a Pentax 6×7 camera. Images of the entrained flow were also obtained to qualify the nature of the counterflowing stream along the upper shear layer

of the jet; the lasers were used to illuminate smoke that was introduced into the ambient gas surrounding the jet. To observe the smoke within the collars, the laser sheet was passed through the lower collar surface, which was manufactured from clear acrylic plastic. The side walls of the collar were also clear to capture the images on film. At the highest operating temperature it was necessary to replace the clear acrylic side walls and lower collar with stainless steel components; the upper collar (including pressure tap arrangement) was unaffected by these changes.

Nonintrusive measurements of the velocity field within the collar were made using particle image velocimetry (PIV). To obtain PIV data, the primary jet was seeded with fine aluminum oxide particles (a commercially available particle having a nominal diameter of ~0.3 μm). These were expected to accurately follow the flow at the operating Mach number of 2, except in the immediate neighborhood of shocks where particle lag can be anticipated, as demonstrated by Wishart and Krothapalli.[17] The secondary flow, which was drawn from the laboratory ambient air, was seeded with smoke having an effective particle diameter slightly larger than that of the aluminum oxide (~0.5–1.5 μm). The laser light sheet used to double expose the particles was generated using a Lumonics Nd:YAG laser; images were captured on a Kodak Megaplus 4.2 charge-coupled device camera ($2k \times 2k$ pixel resolution). To accommodate the introduction of the laser sheet with minimal optical distortion and improve the signal-to-noise ratio of the PIV images, the lower collar was removed from the facility and the jet was vectored toward the upper collar. (Pressure distributions on the upper collar surface indicated that the absence of the lower collar surface had no appreciable effect on the performance of the vectored jet.[18]) A delay of ~0.6 μs was used between laser pulses to capture the particle pairs with sufficient resolution and was determined by the magnitudes of the primary and secondary velocities; a rotating mirror was used to bias the particle pairs and thereby eliminate directional ambiguity (further details can be found in the thesis of Forliti[18]).

Preliminary Observations

A base study was conducted to demonstrate the operation of the fluidic vectoring concept in a cold jet at $T_o = 300$ K for a fixed collar geometry having a gap of $G/H = 0.38$. The series of photographs in Fig. 2 were taken in the vector plane of the jet to illustrate the basic operation of the counterflowing nozzle. The images were obtained over the streamwise distance of approximately 7–$23H$ and were captured by illuminating the jet with a 5-ns exposure of the laser sheet. When the vacuum system, connected to the upper collar, is deactivated and air is allowed to entrain freely into both the upper and lower shear layers, the jet exhausts along its geometrical axis as shown in Fig. 2a. Under these conditions the collar arrangement operates analogously to a jet ejector configuration, albeit inefficiently due to the rapid divergence of the collar walls. Because of the pumping of fluid between the jet and collar, the static pressure in the secondary stream registers a slightly negative value of $P_G = -6.8$ mbar. (To accommodate the introduction of the laser sheet, the lower collar surface was removed from the facility. This resulted in subtly different entrainment characteristics between the upper and lower shear layers of the jet, giving rise to very slight upward vectoring seen in Fig. 2a.)

When the vacuum system is activated, creating counterflow in the gap between the jet and the collar, thrust vectoring can be achieved as shown by the photographs in Figs. 2b and 2c. The static pressure in the gap of the counterflowing stream was reduced from $P_G = -0.061$ bar in Fig. 2b to -0.29 bar in Fig. 2c, corresponding to vector angles estimated from the photographs of 6 and 16 deg, respectively. The jet could be vectored toward either the upper or lower collar by activating the appropriate vacuum system, but all results were obtained with the jet vectored upward to reduce the possibility of damage to the lasers and optical components that were positioned below the jet.

Normalized collar static pressures obtained at $T_o = 300$ K for a gap of $G/H = 0.38$ are shown in Fig. 3. The pressure distributions vary smoothly from the jet exit to the downstream extent of the collar and approach atmospheric pressure as expected. The pressure distributions in Fig. 3 were integrated to obtain the resultant forces

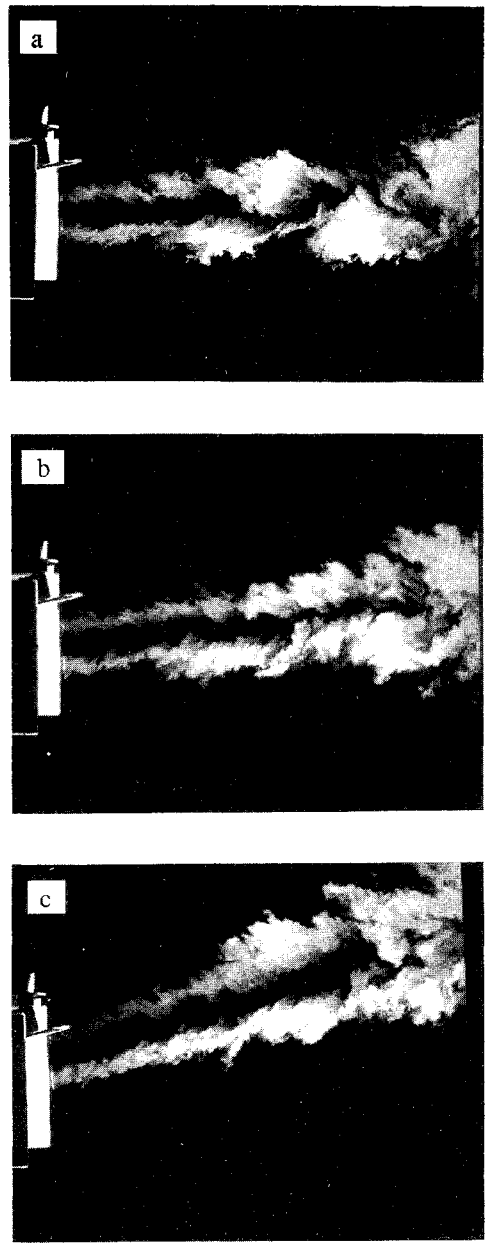

Fig. 2 Condensation photographs of the jet centerplane showing thrust vectoring at a) 0, b) 6, and c) 16 deg using a collar gap height of G/H = 0.38 and T_o = 300 K.

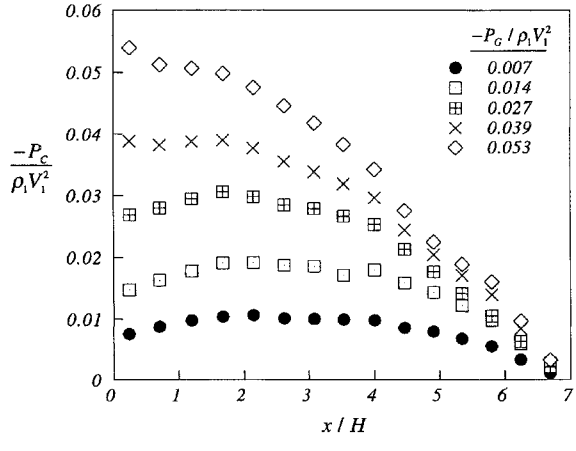

Fig. 3 Collar static pressure distributions taken at T_o = 300 K and G/H = 0.38.

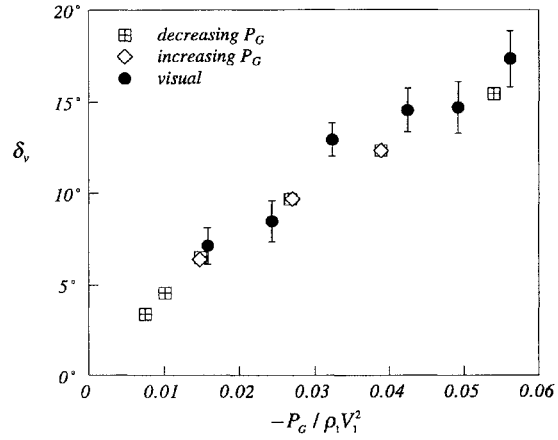

Fig. 4 Thrust vector response curve at T_o = 300 K and G/H = 0.38. Open and solid symbols were obtained from control volume and visual estimates, respectively.

acting on the collar surface. These integral estimates were used in a two-dimensional control volume analysis to evaluate the effective angle of the vectored thrust. Estimates of the momentum flux developed in the secondary stream $\dot{m}_2 V_2$ were required to complete the balance, as well as assumptions regarding the static pressure distribution developed in the exit plane of the primary jet and the gap of the counterflowing stream. The secondary velocity V_2 was approximated by assuming the measured mass flow rate $\dot{m}_2$ was distributed uniformly across the gap between the primary jet and the collar wall. The jet exit plane pressure was determined by the nozzle pressure ratio, and the gap pressure was assumed to be a constant value equal to P_G. Viscous drag was not included in the calculations. Employing these assumptions, the effective thrust vector angle of the jet was estimated using the expression $\delta_v = \tan^{-1}(R_y/R_x)$, where R_x and R_y are the net axial and side forces acting on the nozzle–collar assembly. The control volume analysis also provides the thrust coefficient defined as $C_T = \sqrt{(R_x^2 + R_y^2)}/\dot{m}_1 V_1$, which indicates the magnitude of the losses associated with the turning of the flow.

The control volume predictions of δ_v were compared with the angles measured graphically from a series of photographs similar to those provided in Fig. 2. These comparisons can be seen in Fig. 4, where the abscissa indicates the secondary stream gap pressure normalized by the primary stream momentum flux $\rho_1 V_1^2$. Uncertainty estimates of the graphically determined angles were made by distributing sets of photographs at nominally identical conditions to four individuals and applying a t-test at a 95% confidence interval. A series of tests was also run to examine whether hysteresis could be identified with the operation of the fluidic nozzle. This was accomplished by recording the collar static pressure distributions as the thrust vector angle was first increased and then decreased. As the data in Fig. 4 indicate, no appreciable directional dependence could be identified for the geometry under consideration (G/H = 0.38); hysteretic effects were observed under a limited set of flow conditions for the narrowest gap studied (G/H = 0.27) as discussed later. The thrust vector response curve in Fig. 4 predicts a nearly linear relationship between thrust vector angle and normalized gap pressure over the range of conditions studied. The agreement between the predictions of δ_v from the control volume analysis and the flow visualization studies suggests that the assumptions employed in the momentum balance of the nozzle–collar system are reasonable.

Parametric Effects

The potential advantages of fluidic-based thrust vector control can only be realized if the collar assembly is sufficiently streamlined and lightweight. This design goal must be balanced against the physical requirement that a finite collar surface is essential to take up the side loads demanded during thrust vectoring. This requires an optimization of the nozzle–collar geometry including slot height G, collar length L, and the collar lateral extent given by C. Although an exhaustive parametric analysis of the collar assembly was considered to be beyond the scope of this investigation, the effect of secondary flow slot height G could be readily accommodated in the existing facility and was used to assess whether a minimum slot height could be identified. Furthermore, to evaluate the performance of counterflow thrust vectoring under actual operating conditions, the concept was studied at elevated primary stream stagnation temperatures. We begin this section by addressing the geometric effects, then briefly describe the influence of jet temperature, and conclude with a discussion of the overall thrust vector performance using a scaling parameter that is proposed to further refine collar design.

Effect of Gap Height

The counterflow collars were designed to accommodate variations in gap height over a range of G/H between 0.27 and 0.73. This was done by translating the upper and lower collars in the vertical plane without variation in the collar contour or length. Care was taken during these experiments to position the collars symmetrically about the jet axis and to seal them to the side plates to minimized leakage between the upper and lower jet shear layers. Static pressure distributions on the collar surface are shown in Fig. 5 for the unheated Mach 2 jet operated at counterflow conditions corresponding to $-P_G/\rho_1 V_1^2 \approx 0.041$. The pressure distributions are relatively insensitive to gap height for G/H between 0.38 and 0.73, falling on a smooth curve reminiscent of the trends reported in Fig. 3. Estimates of the thrust vector angle obtained using the data for G/H greater than 0.38, applying the control volume analysis, provide $\delta_v = 14.0 \pm 0.6$ deg at 95% confidence. Collar pressure distributions obtained at other values of $-P_G/\rho_1 V_1^2$ (summarized in Fig. 9 to be discussed later) indicate that the resultant thrust vector angle is not significantly affected by the gap height at least over the range of $0.38 \leq G/H \leq 0.73$. This is primarily because the secondary flow slot height G in the present geometry is small relative to the axial projection of the collar surface itself, which is given by the dimension C in Fig. 1. The effect of slot height will have a more profound influence on thrust vector performance as the collar is made more aerodynamically streamlined, i.e., as C is reduced.

A closer examination of the nozzle operation at G/H = 0.27 provides some insight into the disparate behavior observed for very narrow collar gaps. The collar pressure distributions in Fig. 6, obtained at $-P_G/\rho_1 V_1^2$ = 0.04 and 0.056 are similar to those observed in Figs. 3 and 5. However, when the gap pressure is further reduced, the jet becomes unsteady and displays random variations in visual deflection angle between ~15 and 25 deg. If the gap pressure is reduced further, to $-P_G/\rho_1 V_1^2$ = 0.073, this violent jet behavior is suppressed and steady thrust vectoring at $\delta_v \approx 25$ deg can be observed, giving rise to the collar pressure distribution indicated by the solid symbols in Fig. 6. These observations suggest that the jet becomes attached to the collar surface at sufficiently low vacuum conditions and is supported by the local minimum in the normalized static pressure distribution in the neighborhood of $x/H = 4.5$, where jet impingement can be expected. Measurements of $\dot{m}_2$ indicate that the secondary mass flow is virtually shut off under these conditions, which would be expected during jet attachment. Finally, the operation of the nozzle at lower vacuum pressures

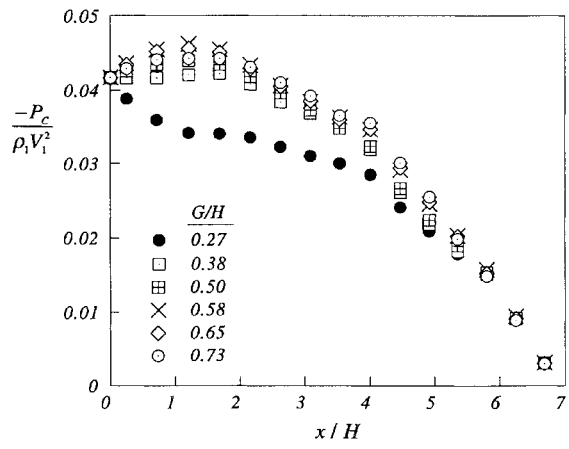

Fig. 5 Collar static pressure distributions as a function of gap height at T_o = 300 K.

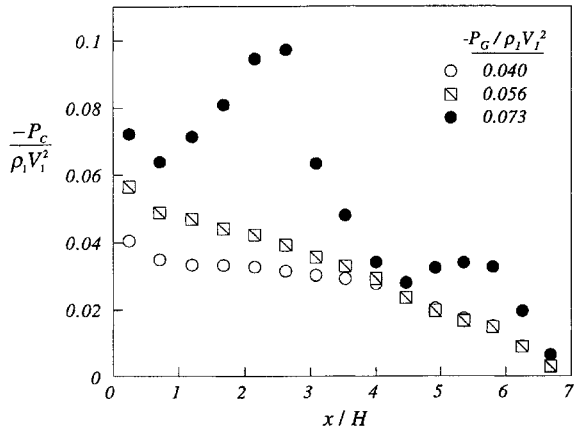

Fig. 6 Collar static pressure distributions taken at a gap height of $G/H = 0.27$ and $T_o = 300$ K.

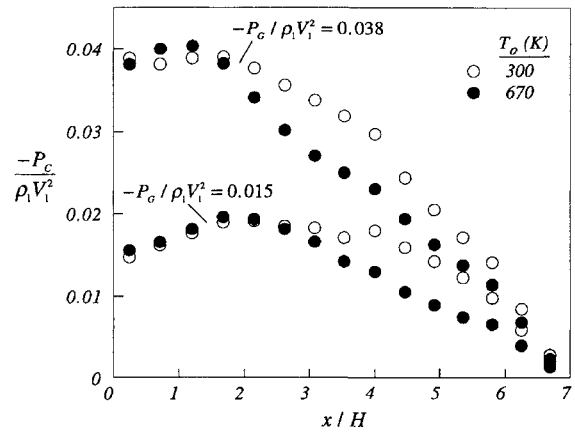

Fig. 7 Collar static pressure distributions taken at $G/H = 0.38$ as a function of jet stagnation temperature.

than $-P_G/\rho_1 V_1^2 = 0.073$ did not result in further increases in δ_v, indicating that the thrust vector angle is constrained by the collar geometry, which in the present study provided a maximum angle given approximately by $\alpha \approx 26$ deg.

A more complete study of counterflow thrust vectoring at small gap heights is required to resolve these preliminary observations of jet unsteadiness and attachment. Certainly, nozzle operation under jet attached conditions would make counterflow thrust vectoring an unlikely candidate for aircraft control applications. However, since reductions in the gap height would be desirable from the standpoint of minimizing the scale of the nozzle–collar assembly, and thereby external drag, a more complete examination of these issues is warranted. Also, since higher vacuum pressures must be maintained during jet attachment, relative to continuous vectoring, it may be possible to avoid attachment by designing a vacuum system that cannot support these pressure levels. These and other issues related to jet attachment are currently under investigation in our laboratory and will be reported at a later time. The remainder of this paper will be devoted to those conditions where steady and nonhysteretic thrust vector performance was observed.

Effect of Primary Jet Temperature

To assess the viability of thrust vector control at realistic jet operating temperatures, a performance study was done in the Mach 2 jet at an elevated stagnation temperature of 670 K. Typical response curves of a hot supersonic jet to counterflow, compared with matched conditions in the cold jet, are shown in Fig. 7 for a gap height of $G/H = 0.38$. Pressure distributions taken at $-P_G/\rho_1 V_1^2 = 0.015$ and 0.038 are in very close agreement for hot and cold operating conditions over the forward third of the collar. However, near $x/H \approx 2$, the heated jet data deviate from the unheated data leading to slightly lower sustainable vacuum pressures on the collar surface and reduced angles of vectored thrust. Estimated values of δ_v were 6.4 and 5.6 deg for cold and hot flow, respectively, at $-P_G/\rho_1 V_1^2 = 0.015$; for operation at $-P_G/\rho_1 V_1^2 = 0.038$ the resultant thrust vector angles are 12.3 and 10.9 deg, respectively.

The thrust coefficients C_T of the hot and cold jets are compared in Fig. 8 over the full range of vacuum pressures investigated for gap heights of $G/H = 0.38$ and 0.58. As expected, the thrust coefficient decreases from unity as the counterflow is first activated and appears to asymptote to a value of $\approx$0.96 as δ_v approaches 16 deg. The thrust coefficient also decreases as the gap height is increased since an axial thrust penalty must accompany the negative gap pressure imposed on a larger gap area. Despite the slight differences in the pressure distributions of Fig. 7, the thrust coefficient indicates that thrust loss is not a strong function of jet stagnation temperature, at least over the moderate temperature range examined in this study.

The subtle variations in the pressure distributions between the hot and cold jet are most likely due to differences in the mixing layer dynamics of the two flows, which depend on the velocity ratio, density ratio, and convective Mach number of the shear layer. As the primary flow is heated from 300 to 670 K the convective

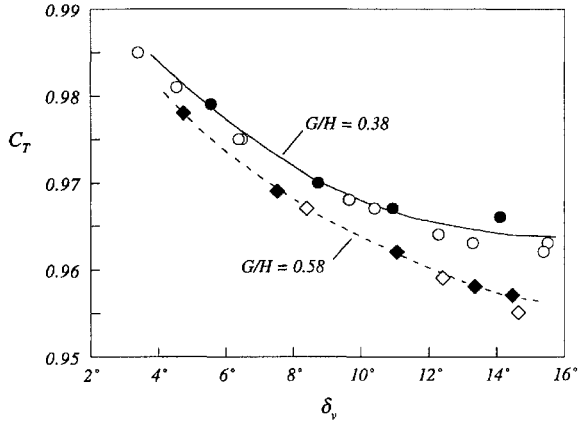

Fig. 8 Thrust coefficient in cold jets (open symbols) and hot jets (solid symbols) for various collar gap heights.

Mach number M_c of the jet shear layer increases from 0.85 to 1.05, where $M_c = (V_1 - V_2)/(a_1 + a_2)$. The effect of compressibility is comparable at these convective Mach numbers, but the effect of density ratio would account for spatial growth rates roughly 20% higher in the shear layer of the heated jet,[13] which presumably will affect the development of the cross-stream pressure gradient near the collar surface necessary for vectoring. Establishing the physical connection between the shear layer characteristics and the pressure distribution on the collar surface motivated a study of the velocity field near the jet exit and is the subject of the next section.

The relationship between δ_v and the normalized gap pressure is provided in Fig. 9, showing the parametric effects considered in this study. Estimates of δ_v are included from the control volume analysis as well as from flow visualization studies, where open and closed symbols correspond to measurements made in cold and hot jets, respectively. The data essentially collapse onto a single curve without any discernible dependence on gap height and only a weak trend indicating that the hot jet requires slightly larger vacuum pressures compared with cold jets to attain similar values of δ_v. The pressure parameter $\hat{P} = (-P_G/\rho_1 V_1^2) \cdot (L/H)$ does a reasonable job of collapsing the thrust vector response data for Mach 2 jets operated at their design pressure ratio of 7.82. The pressure parameter is proportional to the leading order term from the control volume analysis used to evaluate δ_v from measurements of surface pressures and primary/secondary stream momentum fluxes. The minimal scatter in the data of Fig. 9 reflects the fact that the shapes of the collar pressure distributions are reasonably similar (e.g., see Figs. 3, 5, and 7) and that the secondary stream momentum flux is quite small (see the following discussion).

The scaling on $\hat{P}$ can also be argued from momentum considerations of a two-dimensional jet having a thickness H and turning over a radius of curvature R. The pressure gradient across a curved

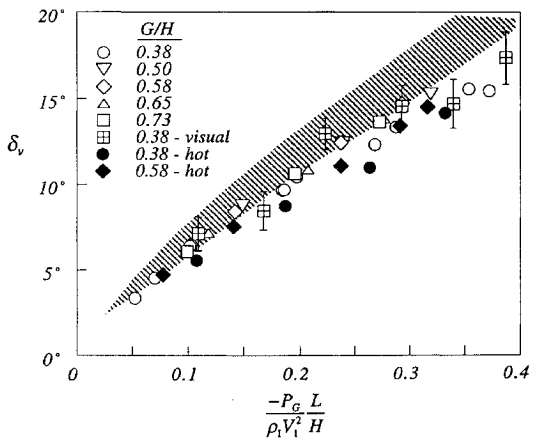

Fig. 9 Thrust vector performance for supersonic jets (symbols) and subsonic jets (shaded region).

stream tube can be estimated from $\partial P/\partial r = \rho u^2/r$, when $\partial P/\partial r$ is approximated by $\Delta P/H$, where $\Delta P\ (= -P_G)$ is the pressure difference across a stream of thickness H. Correspondingly, $\rho u^2/r$ can be estimated as $\rho V_1^2/R$ for a stream having uniform velocity V_1 and experiencing a radius of curvature R. If the jet vectors at an angle δ_v, along a curved surface where $L = R \cdot \sin(\delta_v)$, then we can write $\sin(\delta_v) = (-P_G/\rho_1 V_1^2) \cdot (L/H)$, which is essentially the scaling seen in Fig. 9. The choice of $\hat{P}$ as the independent parameter is advantageous for collar design because it depends only on the gap pressure P_G and not on the entire collar static pressure distribution, which would not likely be known a priori.

The results of Fig. 9 obtained at Mach 2 were compared with subsonic studies of counterflow thrust vectoring performed by Van der Veer,[19] where Mach numbers between 0.2 and 0.5 were examined in a 4:1 aspect ratio rectangular jet. The shaded region in Fig. 9 indicates the approximate scatter of the subsonic data of Van der Veer, which is comparable to the scatter observed in the present supersonic measurements. The subsonic jet experiments included the effects of gap height G/H and collar length L/H, as well as the primary jet momentum flux $\rho_1 V_1^2$ (the latter two of which were not independently varied in the present study), providing evidence that $\hat{P}$ is an appropriate scaling parameter for jets operated near their design pressure ratios. There is a discernible trend in the data suggesting that lower gap pressures are required as the primary stream Mach number is increased to achieve a particular value of δ_v. It is likely that the lower side forces developed in supersonic jets with counterflow are due to reduced entrainment rates, relative to the jet momentum flux $\rho_1 V_1^2$, as the Mach number is increased.

Finally, to assess the efficiency of the thrust vector control, the secondary mass flow was measured under hot and cold primary jet conditions for a limited variation in gap height. Here we were interested in obtaining estimates of the mass flow ratio $\dot{m}_2/\dot{m}_1$ as well as the power requirements necessary for fluidic control. Within the measurement uncertainty, estimates of $\dot{m}_2/\dot{m}_1$ were insensitive to gap pressure as well as jet stagnation temperature. For instance, at $G/H = 0.38$, the magnitude of $\dot{m}_2/\dot{m}_1$ was a nearly constant value of 0.02 for values of $\hat{P}$ between 0.1 and 0.4, and jets operating at stagnation temperatures between 300 and 670 K. In the present configuration the pumping power needed to drive the secondary flow along the collar surface can be given approximately by $\dot{m}_2 P_G/\rho_2$. The 2% secondary mass flow requirement, given earlier, corresponds to an auxiliary power of 0.7 and 0.3% of the primary jet power for the cold and hot jets, respectively. The secondary mass flow requirements did, however, depend nearly proportionally on the gap height itself, taking values of $\dot{m}_2/\dot{m}_1 \approx 0.02$ and 0.03 for gap heights of $G/H = 0.38$ and 0.58, respectively. This would suggest that the velocity ratio V_2/V_1 plays an important role in determining the shear layer dynamics during thrust vectoring.

Velocity Field Study Using PIV

A physical understanding of the connection between the shear layer dynamics and the collar surface pressures requires that the flowfield be examined in the neighborhood of the jet exit and in the vicinity of the collar surface. Since intrusive measurements tended to alter the vector angle itself—due to the feedback generated by the edge tone emitted when a physical probe was placed in the shear layer[18]—a nonintrusive measurement technique was required. PIV has been used successfully in previous supersonic free jet studies, and the comparisons between the velocities as measured by PIV and intrusive probes show excellent agreement.[20,21] PIV measurements were made in the Mach 2 jet for thrust vector control under three conditions, corresponding to $-P_G/\rho_1 V_1^2 = 0.006$, 0.024, and 0.051. These studies will be referred to as the unvectored, moderately vectored, and maximum vectored cases, respectively. The time-averaged velocity vector fields reported next (Figs. 10, 11, and 14) were obtained by averaging 90 instantaneous PIV images. The gap height was fixed during these studies at $G/H = 0.38$ and the jet was unheated ($T_o = 300$ K).

The first case that will be discussed ($-P_G/\rho_1 V_1^2 = 0.006$) occurs when the vacuum system is entirely disconnected from the collar assembly. The slightly negative static pressure developed in the collar gap is caused by the pumping effect of the shear layers. Figure 10 shows the resulting mean velocity vector field and corresponding isovelocity (magnitude) contours. The solid and dashed lines in the isovelocity plots correspond to forward and reverse flowing fluid, respectively. It can be seen that counterflow is generated in the region between the upper shear layer and the collar wall due to jet entrainment. This naturally induced counterflow is quite high, on the order of 25–30% of the primary jet velocity, in the region approximately midway along the collar (i.e., at $x/L \approx 0.5$). The jet is essentially unvectored in Fig. 10, with only slight differences in the upper and lower shear layers, owing to the fact that the lower collar surface was removed during the PIV study to accommodate the introduction of the laser sheet.

The velocity vector fields and isovelocity contours are useful for visualization of shock cell structure within the jet (also see Figs. 11 and 14). The potential core appears to have minimal spatial velocity variations due to the weak nature of the expansion and compression waves present. This wave structure is caused by the slightly underexpanded flow on the upper side of the jet resulting when free entrainment is inhibited by the placement of the collar surface. The spacing of the shock cells is roughly $3H$, which is in agreement with the cell spacing of a very slightly underexpanded Mach 2 rectangular

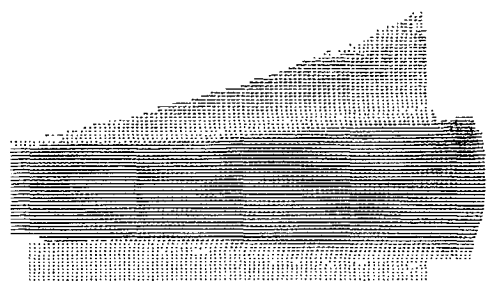

a) Time-averaged velocity vector field

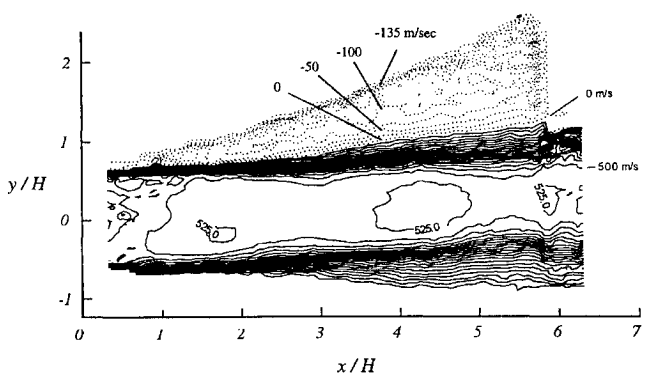

b) Isovelocity contours

Fig. 10 PIV results for an unvectored jet at $G/H = 0.38$ and $T_o = 300$ K.

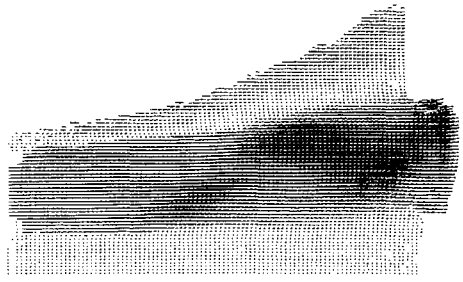

a) Time-averaged velocity vector field

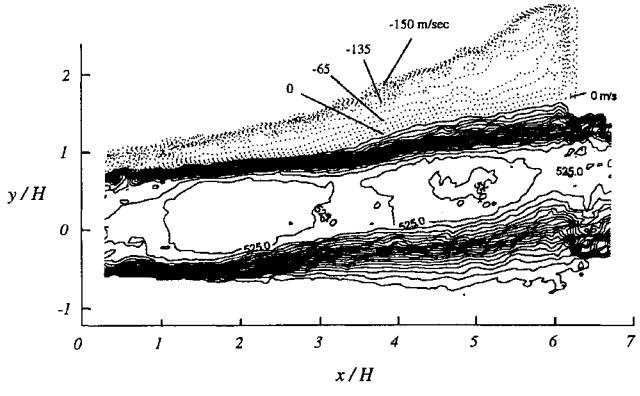

b) Isovelocity contours

Fig. 11 PIV results for a moderately vectored jet ($-P_G/\rho_1 V_1^2 = 0.024$) at $G/H = 0.38$ and $T_o = 300$ K.

free jet. The agreement found in the potential core mean velocity between the free jet (no collars) and the unvectored case (with collars) suggests the addition of the collar itself has a minimal effect on the expansion characteristics of the jet.[18]

The mean velocity field for the moderately vectored jet is shown in Fig. 11. The primary flow turns toward the upper collar and leaves the measurement domain vectored at $\delta_v \approx 8$ deg as determined by averaging the velocities contained within the potential core. This approach for determining δ_v was relatively insensitive to the precise definition of the potential core as described by Forliti.[18] Owing to the greater underexpansion on the upper side of the jet (the exit static pressure on the top side of the jet is below atmospheric pressure by ~2.5% of the jet dynamic pressure), the velocity magnitude within the potential core displays larger spatial variations than the unvectored case. An expansion fan emanates from the upper jet lip and intersects the lower shear layer at an angle of 30 deg as expected for flow at Mach 2. The waves are then reflected from the lower shear layer as a weak oblique shock to accommodate the pressure matching condition of the free shear layer. This oblique wave can be clearly seen in the velocity vector plot of Fig. 11a, originating in the lower shear layer at $x/H \approx 2.5$.

To determine the influence of gap pressure on the induced secondary flow, the velocity ratio across the upper shear layer of the jet was evaluated from the PIV data. To obtain a representative value of the velocity in the secondary stream, the maximum velocity magnitude was taken and normalized by the primary jet exit velocity V_1. The axial variations in velocity ratio, shown in Fig. 12, indicate some scatter but provide a reasonably accurate picture of the counterflowing velocity field sustained in the neighborhood of the collar surface. The most distinguishing feature of the velocity ratio distributions is seen over the first $3H$ downstream of the jet exit, where the levels of counterflow are significantly higher for the moderately vectored jet. In the unvectored case, the large secondary velocities (~150 m/s), which are reached near the midpoint of the collar, decrease rapidly toward the jet exit as the mass in the counterflowing stream is entrained by the primary jet and carried downstream. In the moderately vectored case, the secondary mass flows that are present at the collar midpoint are sustained closer to the jet exit, although the actual mass that is drawn into the vacuum system is quite modest. Measurements of the mass flow drawn through the

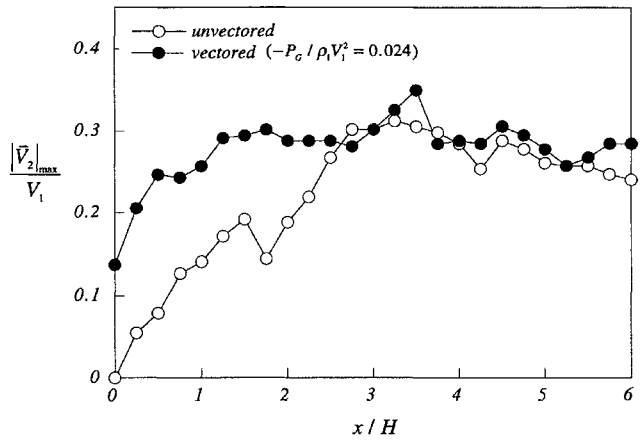

Fig. 12 Velocity ratio distribution along the upper shear layer for T_o = 300 K and $G/H = 0.38$.

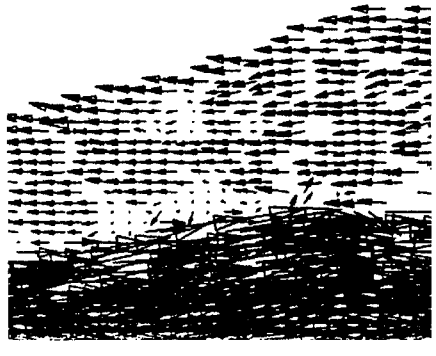

a) Unvectored jet

b) Moderately vectored jet ($-P_G/\rho_1 V_1^2 = 0.024$)

Fig. 13 Instantaneous PIV velocity vector field over a streamwise distance of $2 < x/H < 4.5$ at $G/H = 0.38$ and $T_o = 300$ K.

vacuum system revealed that $\dot{m}_2$ was only 2% of $\dot{m}_1$, indicating that the average secondary velocity at $x/H = 0$ is approximately 9.5% of the primary jet velocity compared with a maximum magnitude of 14% measured using PIV as shown in Fig. 12.

The shear layer structure was examined by capturing instantaneous PIV images of the flow in a region extending from $2H$ to $4.5H$ downstream of the jet exit for the unvectored and moderately vectored cases. This region was selected to be far enough downstream of the jet exit to view the layer when it was relatively thick but also close enough to capture the flow where differences in velocity ratio were observed (see Fig. 12). Representative velocity vector plots of the instantaneous flow structure, shown in Fig. 13, indicate a distinct difference in the shear layer structure before and after vectoring (images were selected randomly). The natural entrainment in the unvectored case is accomplished with surprisingly little flow structure in the upper shear layer as seen in Fig. 13a. When the gap pressure is reduced and the jet is vectored, the shear layer displays relatively large structures as seen in Fig. 13b. But despite

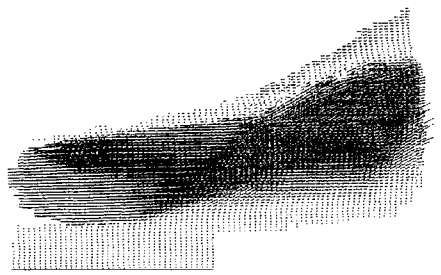

a) Time-averaged velocity vector field

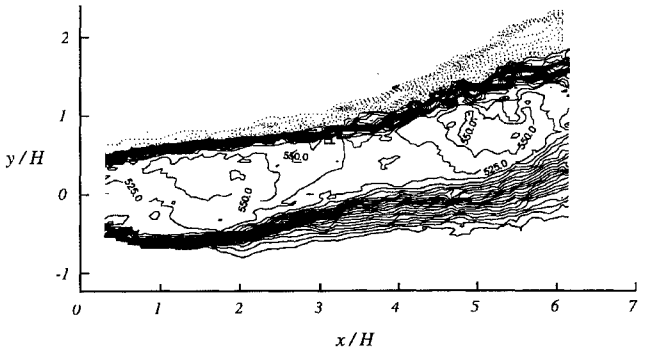

b) Isovelocity contours

Fig. 14 PIV results for maximum vectoring conditions ($-P_G/\rho_1 V_1^2$ = 0.051) at G/H = 0.38 and T_o = 300 K.

the appearance of these large-scale structures, a comparison of the time-averaged flowfield of the unvectored jet (Fig. 10) to the moderately vectored jet (Fig. 11) suggests that these structures do not lead to significant spreading on the high-speed side of the shear layer. This implies that the structures reside essentially on the low-speed side of the layer, i.e., in the secondary stream, a conclusion that was reinforced by studying many instantaneous images of the shear layer such as those shown in Fig. 13. (Additional random images can be found in the thesis of Forliti.[18])

The time-averaged shear layer behavior observed at maximum vectoring conditions ($-P_G/\rho_1 V_1^2 = 0.051$) is shown in Fig. 14. Again, one can see that the high-speed side of the upper shear layer is quite thin relative to the unvectored case (Fig. 10). Instantaneous images of the shear layer structure (not shown here) are reminiscent of the flow patterns seen in Fig. 13b, indicating that the structures reside to a great extent in the low-speed portion of the layer. The velocity vector plot clearly shows the turning of the flow up to $\delta_v \approx 15$ deg as well as the wave structure described early. The oblique shock that originates from the lower shear layer can be seen to intersect the upper shear layer in the isovelocity plot of Fig. 14b. The shock/shear layer interaction that occurs at $x/H \approx 4$ leads to flow turning as expected. Although thrust vectoring in supersonic jets is assisted by the formation of shocks, the presence of shocks is not a necessary prerequisite for vectoring as demonstrated by the effectiveness of the technique when applied to subsonic flows.[19]

One final point we would like to make concerns the origin of the fluid in the secondary stream. Because of the intense mixing that occurs in the shear layer of the vectored jet, it is not obvious whether the secondary flow drawn into the vacuum system originates primarily from the ambient fluid or from the primary jet itself. To address this question the ambient air was seeded with smoke and the primary jet was heated slightly to $T_o = 400$ K ($G/H = 0.38$). Heating the primary flow eliminated condensation and allowed only the entrained flow to be illuminated by the laser sheet. The image captured in Fig. 15, for maximum vectoring conditions, shows the smoke originating above the collar and being drawn into the collar housing as well as being entrained by the primary jet. It is clear that smoke penetrates along the entire secondary flow path, eliminating the possibility that the flow entering the vacuum system originates entirely from the primary jet. The precise fraction of the primary jet flow that is extracted by the secondary stream is currently unknown

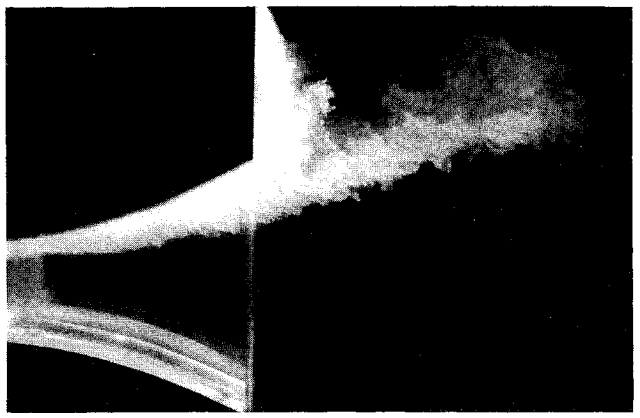

Fig. 15 Flow visualization of the side view of the jet when smoke is entrained into the upper shear layer. The collar gap is G/H = 0.38, T_o = 400 K, and $-P_G/\rho_1 V_1^2$ = 0.055.

but in any event must be small since the total secondary mass flow is less than approximately 2% of the primary jet flow.

Discussion

The results presented thus far provide an encouraging picture of the role that counterflow may have in modern aircraft that employ vectored thrust nozzles. In particular, we anticipate that the characteristics of the countercurrent mixing layer play an important function in determining the jet dynamics in the collar region. This expectation is drawn, in part, from our earlier studies of countercurrent shear flows[13–15] as well as the present PIV results indicating the existence of large structures in the jet shear layer when counterflow is applied. Based on these findings, we can provide a preliminary physical description of the operating principle upon which the counterflow thrust vectoring technique is based.

When the gap pressure P_G is reduced on one side of the rectangular jet, a secondary reverse flowing stream is created between the primary jet and the adjacent collar surface. The maximum velocity magnitude of this secondary stream is nearly 30% of the primary jet velocity and can be maintained over a significant portion of the shear layer. The effect of reducing P_G is to increase the magnitude of the velocity ratio across the shear layer in the vicinity of the jet exit, which in turn is responsible for the formation of large structures in the shear layer during thrust vectoring. The dynamics of the upper shear layer are complicated by two competing tendencies: on the one hand the large structures will facilitate the entrainment of ambient fluid and draw larger secondary flows along the collar surface toward the jet exit; on the other hand, these same structures will inhibit the passage of flow in the secondary stream, creating a pressure drop along the collar surface. It is this pressure drop that allows vacuum conditions to be maintained on the collar surface and is responsible for generating the side loads necessary for vectoring the thrust. Developing a larger pressure drop along the collar, for instance, by roughening the collar surface, may further enhance the vectorability of the jet while minimizing the secondary flow requirements needed for actuation.

The proximity of the high momentum fluid of the primary jet (i.e., the outer edge of the jet potential core) to the collar wall will approximately define the flow path of the secondary stream. As the jet temperature is increased, the shear layer will spread more quickly, and as a result, the high momentum fluid of the jet potential core will be displaced away from the collar surface. Hence, for a fixed $\dot{m}_2$, the effect of heating the jet will be to increase the effective area through which the secondary flow can pass. This will lead to a lower pressure drop along the secondary flow path and reduce the side forces available for vectoring thrust. This was the trend observed in Fig. 7 when the jet was heated from 300 to 670 K. Presumably the collar shape can be redesigned to counteract this effect and increase the effective thrust vector angle for a given gap pressure P_G.

Continuous control of the thrust vector angle can be attained in principle because the dynamics of the shear layer structures, and

therefore entrainment rate, are a function of velocity ratio.[13] However, one potential limitation of the nozzle–collar arrangement is the attachment of the primary jet to the collar, leading to a hysteretic response. Under these conditions the thrust vector angle would be fixed, leading to a loss of control. Presumably hysteresis can be prevented for particular nozzle–collar geometries for the following reason. As the jet is drawn off axis, the cross-sectional area between the collar and the jet is reduced, leading to an increased pressure drop in the counterflowing stream. Eventually, the proximity of the primary jet to the wall will tend to choke the secondary flow, eliminating the mechanism needed to sustain the flow structure and entrainment. In principle, an equilibrium position will be achieved where sufficient secondary flow is present to disturb the layer and cause jet vectoring, but not too large a vector angle such that the counterflow is cut off. Jet attachment conditions can only be maintained if sufficient vacuum pressure is present in the absence of counterflow to hold the jet against the collar. We believe this situation exists for the smallest collar gap height investigated of $G/H = 0.27$ for $-P_G/\rho_1 V_1^2 = 0.073$, as discussed in conjunction with Fig. 6.

Conclusions

In summary, it has been shown that the thrust of supersonic rectangular jets can be effectively pitch vectored up to 16 deg by employing a fluidic counterflowing nozzle. The performance of the nozzle system is relatively insensitive to jet stagnation temperature, at least over the range examined here, and the thrust vector angle is approximately a linear function of the static pressure developed in the counterflowing stream. The principal advantage of the fluidic approach is the elimination of aerodynamic control surfaces and the associated control hardware, which can add considerable weight and maintenance requirements to the aircraft. The fluidic design also has the potential benefit of film cooling inherent to the cold counterflowing stream between the hot primary jet and the collar surface. Design considerations used in future optimization of the nozzle–collar geometry must seek to minimize the external drag of the collar assembly as well as the pump work required to develop the secondary flow. Furthermore, the role of external flow must be examined to determine the influence of flight conditions on the pressure distribution of the collar surface. The external contour of the nozzle–collar housing will determine the pressure boundary condition at the downstream extent of the collar and therefore the secondary flow that can be developed between the primary jet and the collar wall.

Acknowledgments

The authors would like to express their thanks to the Office of Naval Research (Contract N00014-92-J-1406) and the U.S. Air Force Office of Scientific Research (Contract F49620-92-J-0426) for financial support of this research. We also benefited considerably from discussions with F. Alvi and the assistance of M. Van der Veer, C. Ross, and C. J. King.

References

[1]Doonan, J. G., and Kuchar, A. P., "Scale Model Test Results of a Multi Slotted 2-D/C-D Ejector Nozzle," AIAA Paper 92-3264, July 1992.

[2]Snow, B. H., "Thrust Vectoring Control Concepts and Issues," Society of Automotive Engineers, SAE Technical Paper Series, 901848, Warrendale, PA, 1990.

[3]Capone, F., Smereczniak, P., Spetnagel, D., and Thayer, E., "Comparative Investigation of Multiplane Thrust Vectoring Nozzles," AIAA Paper 92-3264, July 1992.

[4]Olsen, R. E., "Reattachment of a Two-Dimensional Compressible Jet to an Adjacent Plate," *Symposium on Fluid Jet Control Devices*, American Society of Mechanical Engineers, New York, 1962, pp. 23–31.

[5]Comparin, R. A., Glaettli, H. H., Mitchell, A. E., and Mueller, H. R., "On the Limitations and Special Effects in Fluid Jet Amplifiers," *Symposium on Fluid Jet Control Devices*, American Society of Mechanical Engineers, New York, 1962, pp. 65–73.

[6]Warren, R. W., "Some Parameters Affecting the Design of Bistable Fluid Amplifiers," *Symposium on Fluid Jet Control Devices*, American Society of Mechanical Engineers, New York, 1962, pp. 75–82.

[7]Fitzgerald, R. E., and Kampe, R. F., "Boundary Layer TVC for Missile Applications," AIAA Paper 83-1153, June 1983.

[8]Carroll, G. R., and Cox, H., "A Missile Flight Control Cystem Using Boundary Layer Thrust Vector Control," AIAA Paper 83-1149, June 1983.

[9]Porzio, A. J., and Franke, M. E., "Experimental Study of a Confined Jet Thrust Vector Control Nozzle," *Journal of Propulsion and Power*, Vol. 5, No. 5, 1989, pp. 596–601.

[10]Parekh, D. E., Kibens, V., Glezer, A., Wiltse, J. M., and Smith, D. M., "Innovative Jet Flow Control: Mixing Enhancement Experiments," AIAA Paper 96-0308, Jan. 1996.

[11]Cornelius, K. C., and Lucius, G. A., "Thrust Vectoring Control from Underexpanded Asymmetric Nozzles," AIAA Paper 93-3261, July 1993.

[12]Wallace, D., and Redekopp, L. G., "Flow Vectoring of Two-Dimensional Wakes and Jets," AIAA Paper 94-2219, June 1994.

[13]Strykowski, P. J., Krothapalli, A., and Jendoubi, S., "The Effect of Counterflow on the Development of Compressible Shear Layers," *Journal of Fluid Mechanics*, Vol. 308, Feb. 1996, pp. 63–96.

[14]Strykowski, P. J., and Wilcoxon, R. K., "Mixing Enhancement Due to Global Oscillations in Jets with Annular Counterflow," *AIAA Journal*, Vol. 31, No. 3, 1993, pp. 564–570.

[15]Strykowski, P. J., and Krothapalli, A., "The Countercurrent Mixing Layer: Strategies for Shear-Layer Control," AIAA Paper 93-3260, July 1993.

[16]Clemens, N. T., and Mungal, M. G., "A Planar Laser Mie Scattering Technique for Visualizing Supersonic Mixing Flows," *Experiments in Fluids*, Vol. 11, No. 2/3, 1991, pp. 175–185.

[17]Wishart, D. P., and Krothapalli, A., "On The Structure of a Heated Supersonic Jet," AIAA Paper 94-0666, Jan. 1994.

[18]Forliti, D. J., "Measurement of a Rectangular Mach 2 Jet Under Free and Counterflow Thrust Vectored Conditions," M.S. Thesis, Dept. of Mechanical Engineering, Florida State Univ., Tallahassee, FL, 1995.

[19]Van der Veer, M. R., "Counterflow Thrust Vectoring of a Subsonic Rectangular Jet," M.S. Thesis, Dept. of Mechanical Engineering, Univ. of Minnesota, Minneapolis, MN, 1995.

[20]Ross, C. B., "Calibration of Particle Image Velocimetry in a Shock-Containing Supersonic Flow," M.S. Thesis, Dept. of Mechanical Engineering, Florida State Univ., Tallahassee, FL, 1993.

[21]Wishart, D. P., "The Structure of a Heated Supersonic Jet Operating at Design and Off-Design Conditions," Ph.D. Thesis, Dept. of Mechanical Engineering, Florida State Univ., Tallahassee, FL, 1995.